JMEPEG (2013) 22:1194–1200
DOI: 10.1007/s11665-012-0378-x
©ASM International
1059-9495/$19.00

Microstructure and Properties of Cast B-Bearing High Speed Steel

Hanguang Fu, Shengqiang Ma, Jianqiang Hou, Yongping Lei, and Jiandong Xing

(Submitted February 8, 2012; in revised form August 27, 2012; published online September 18, 2012)

Microstructure, mechanical properties, and wear resistance of B-bearing high-speed steel (HSS) roll material containing 0.90-1.00% C, 1.3-1.5% B, 0.8-1.5% W, 0.8-1.5% Mo, 4.6-5.0% Cr, 1.0-1.2% V, and 0.15-0.20% Ti were studied by means of the optical microscopy (OM), the scanning electron microscopy (SEM), x-ray diffraction (XRD), hardness, impact toughness, and pin-on-disk abrasion tests. The results showed that as-cast structure of B-bearing HSS consisted of α-Fe-, $M_{23}(B,C)_6$-, $M_3(B_{0.7}C_{0.3})$-, and $M_2(B,C)$-type borocarbides, a small quantity of retained austenite, and a small amount of TiC. The hardness and impact toughness values of as-cast B-bearing HSS reached 65-67 HRC and 80-85 kJ/cm^2, respectively. There were many $M_{23}(B,C)_6$-precipitated phases in the matrix after tempering, and then, with increasing temperature, the amount of precipitated phases increased considerably. Hardness of B-bearing HSS gradually decreased with the increasing tempering temperature, and the change of tempering temperature had no obvious effect on impact toughness. B-bearing HSS tempered at 500 °C has excellent wear resistance, which can be attributed to the effect of boron.

Keywords boron alloying, high speed steel roll, metals and alloys, microstructure, solidification, temper treatment

1. Introduction

High-speed steels (HSS), widely applied in high-speed machining and cutting operations, are characterized by excellent hardness, wear resistance, and high-temperature properties (Ref 1, 2). Recently, they have increasingly been used for hot mill work rolls by increasing their carbon and vanadium contents, and were found suitable as replacement for high chromium white cast irons and high Ni-Cr infinite chill irons (Ref 3-6). However, HSS rolls contain many costly alloy elements, such as tungsten, molybdenum, vanadium, niobium, cobalt, etc. and incur higher production cost (Ref 5, 6), restricting the application of HSS rolls.

Boron is an inexpensive element and is widely used in steel (Ref 7-9). Many researches discovered that a small quantity of boron could improve the hardenability and wear resistance of steel (Ref 7, 8). Boron also combined with iron and formed borides of high hardness (such as Fe_2B or Fe_3B), and increased the hardness and wear resistance of cast Fe-B alloy (Ref 8, 9). The aim of the current study is to analyze the effect of boron on microstructures and properties of HSS. We intend to develop a kind of B-bearing HSS roll material that has excellent mechanical properties and wear resistance, with lower production cost.

Hanguang Fu, Jianqiang Hou, and **Yongping Lei**, School of Materials Science and Engineering, Beijing University of Technology, Number 100, Pingle Garden, Chaoyang District, Beijing 100124, People's Republic of China; and **Shengqiang Ma,** and **Jiandong Xing**, State Key Laboratory for Mechanical Behavior of Materials, School of Materials Science and Engineering, Xi'an Jiaotong University, Xi'an 710049 Shaanxi Province, People's Republic of China. Contact e-mail: fhg64@263.net.

2. Experimental

2.1 Specimen Preparation

The alloy used in the present study was melted in a 50 kg-capacity medium frequency induction furnace. Initial charge materials were clean pig iron and steel scrap. Ferroalloys such as Fe-81%W, Fe-55%Mo, Fe-51%V, Fe-62%Cr, Fe-21%B, Fe-32%Ti, and Fe-78%Mn were added to a slag-free molten steel so as to minimize the oxidation loss and the slag formation. The melt was subsequently super-heated to 1620 °C and transferred into a pre-heated teapot ladle. After removal of any dross and slag, the melt was poured at 1480 °C into the metal molds to produce *Y*-block ingot according to Ref 10 and 11. The metal molds were preheated before casting, the preheating temperature was 240 °C, and the preheating time was 3 h. The main chemical compositions (wt.%) of B-bearing HSS are as follows: 0.90-1.00 C, 1.3-1.5 B, 0.8-1.5 W, 0.8-1.5 Mo, 4.6-5.0 Cr, 1.0-1.2 V, 0.4-0.6 Mn, 0.3-0.7 Si, 0.15-0.20 Ti, and $S < 0.035$; $P < 0.035$. Metallurgical samples were cut directly from 10 mm above the bottom of the *Y*-block ingot. The shape and dimension of *Y*-block ingot are shown in Fig. 1.

The tempering treatments of the specimens were carried out in a vacuum furnace with a vacuum limit of 6.7×10^{-2} Pa. The temperatures of tempering treatments were 300, 400, 500, 530, and 560 °C. The duration of holding during the tempering treatments was 4 h, after which the furnace was cooled to room temperature. The tempering cycle was one time.

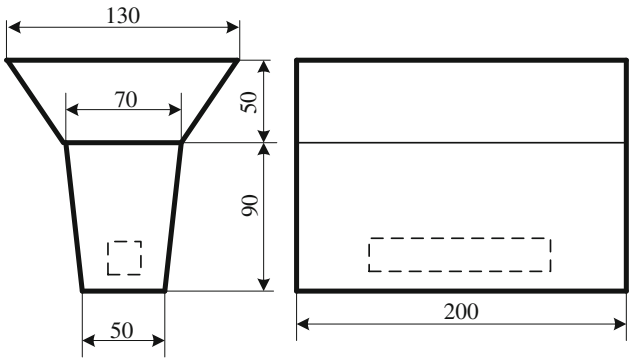

Fig. 1 Shape and dimension of Y-block ingot

Table 1 Values of K between $I_{\alpha(hkl)i}$ and $I_{\gamma(hkl)j}$

Plane of austenite	Plane of martensite	K
(220)	(211)	0.65
(311)	(200)	0.87

2.2 Microstructure Examination

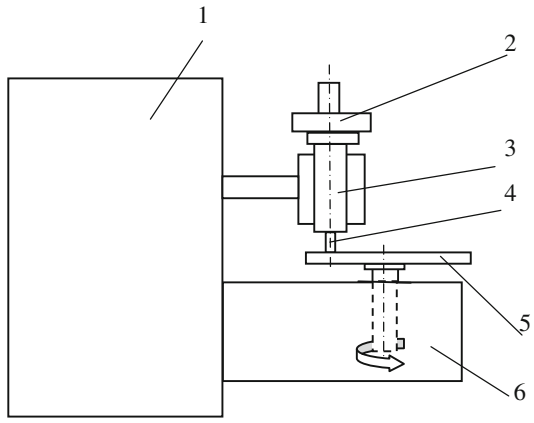

Fig. 2 Schematic drawing of the abrasive wear tester used in this study: 1—controller; 2—load; 3—holder; 4—specimen; 5—disk; and 6—revolver

Investigation techniques used for characterization of B-bearing HSS microstructure included optical microscopy (OM) and scanning electron microscopy (SEM). The samples were etched with 5% nital for OM examination, while a mixture of 5 cc HCl, 45 cc 4% picral, and 50 cc 5% nital was used as an etchant for SEM evaluation. The OM used was a Neophot 32. The SEM used was a JEOL JSM-6100. XRD was performed on the bulk material of B-bearing HSS specimens and was carried on a MXP21VAHF diffractometer with Cu K_α radiation at 40 kV and 200 mA as an x-ray source. The sample was scanned in the 2θ range of 20°-80° in a step-scan mode (0.02° per step). The volume fractions and size of borocarbides were obtained by image analysis using Leica digital images analyzer.

2.3 Hardness and Impact Toughness Tests

The microhardness of borocarbide and matrix in B-bearing HSS were measured by means of a Vickers microhardness tester with a load of 0.5 N as proposed in Ref 12 and 13. Macrohardness measurement of B-bearing HSS was done using an HR-150A-type Rockwell hardness tester. The test load was 150 kg. At least seven indentations were made on each sample under each experimental condition to check reproducibility of the hardness data. Charpy unnotched impact tests were performed at room temperature using a 300 J capacity machine; the dimensions of specimens were 10 mm × 10 mm × 55 mm. The average values from three test specimens are reported here.

The retained austenite content of the matrix was determined using x-ray diffraction (XRD) (Ref 13, 14). A special sample holder, which continuously tilted and rotated the sample, was used to eliminate orientation effects (Ref 15). The results are given as the proportion of austenite in the matrix, based on a direct comparison of the intensity of the γ_{220}, γ_{311}, α_{200}, and α_{211} diffraction peaks according to the Eq 1 (Ref 16, 17)

$$V_\gamma = \frac{1 - V_C}{1 + k\frac{I_{\gamma(hkl)i}}{I_{\gamma(hkl)j}}} \quad \text{(Eq 1)}$$

where V_γ and V_C are the volume fractions of the retained austenite and carbide in the high-carbon HSSs, respectively; thereafter, the carbide volume fraction is obtained by image analysis using Leica digital images analyzer after deep-etching the samples in a solution of ferric chloride. $I_{\alpha(hkl)i}$ and $I_{\gamma(hkl)j}$

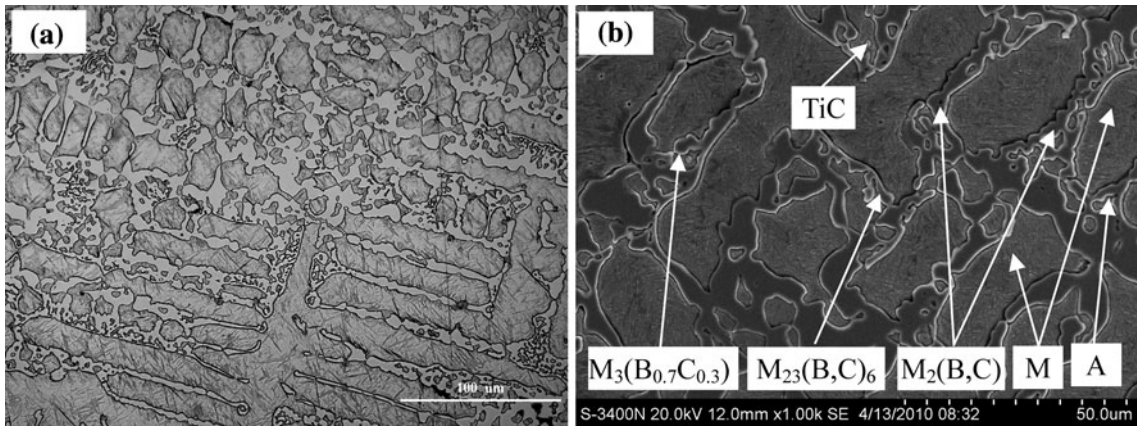

Fig. 3 OM (a) and SEM (b) of as-cast B-bearing HSS. M—Martensite, A—Austenite

are the intensities of the certain crystal planes of martensite and austenite, respectively. K, as shown in Table 1 (Ref 18), is the scale factor between $I_{\alpha(hkl)i}$ and $I_{\gamma(hkl)j}$.

2.4 Sliding Wear Tests

Wear tests were conducted using a conventional pin abrasion testing machine (ML-10). Figure 2 shows a schematic drawing of the pin abrasion testing machine (Ref 19-22). The deadweight of the applied load was 39.2 N. The sliding distance was 16.4 m. The sliding speed was 0.1 m/s. The dimension of disk was 30 mm in diameter and 5 mm in thickness. Silicon carbide (SiC) paper was placed on the disk. The pin samples were abraded on a 280-grit (52 μm) SiC paper, and the hardness of SiC was 2585-2840 Hv. The pin specimen for the pin-on-disk tests was a cylinder, with one end making contact with the abrasive paper on the disk. The pin specimens were 6 mm in diameter and 20 mm in length. Before the experiment, the pin specimens were cleaned with alcohol, and the masses of the specimens were measured gravimetrically with 0.1 mg sensitivity according to Ref 23, 24. Then, they were assembled into the apparatus. Following a "run-in" period, tests were conducted on a fresh sheet of abrasive paper. After one running-in test, three tests wear performed on each specimen. The results of wear tests were the average of three tests. The abrasion rates were calculated according to the following formula (Ref 21, 22, 25, 26):

$$W_a = \Delta G/(\rho \cdot l) \quad \text{(Eq 2)}$$

where, W_a is the abrasion rate (m^3/m); ΔG is the mass loss (mg); ρ is the density (mg/m^3); and l is the sliding distance of the sample, l = 16.4 m.

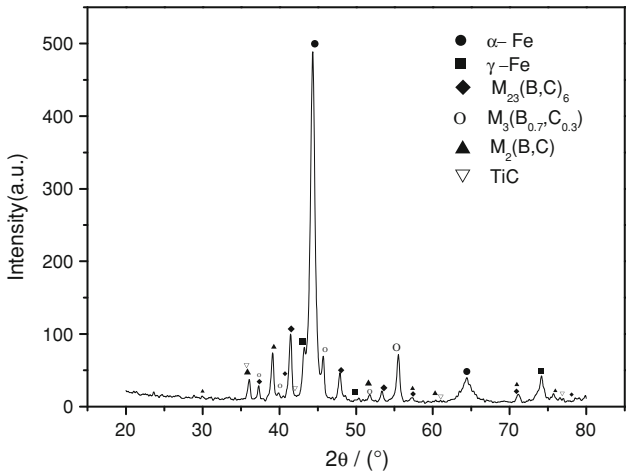

Fig. 4 XRD spectrum of as-cast B-bearing HSS roll material

3. Results and Discussion

3.1 Microstructure and Properties of As-Cast B-Bearing HSS

As-cast structures of B-bearing HSS are shown in Fig. 3. It is different from the as-cast structure of traditional high-carbon high-vanadium HSS roll material, which consists of MC-, M_2C-, and M_7C_3-type carbide and austenite, martensite, and pearlite (Ref 27, 28). The solidification microstructures of B-bearing HSS consist of α-Fe, borocarbides, a small quantity of retained austenite, and small amount of TiC. The XRD pattern of Fig. 4 shows that borocarbides contain $M_{23}(B,C)_6$, $M_3(B_{0.7}C_{0.3})$, and $M_2(B,C)$. Retained austenite was quantified by XRD. The amount of retained austenite is 5.3 vol.%. According to Fe-B binary phase diagram (Ref 29), the solid solubility limit of boron in γ-Fe is 0.02 wt.%, which leads to the enrichment of boron at grain boundary and the formation of borocarbides along the grain boundary. Moreover, the volume fractions and size of borocarbides in B-bearing HSS are $23.8 \pm 1.0\%$ and 3.4 ± 0.8 μm, respectively, in which the numbers after "±" indicate the standard deviation from the mean of the analyses done on five fields at least. The microhardness of matrix is 950-1000 Hv, which indicates that α-Fe of as-cast B-bearing HSS is martensite. As a rule, in as-cast HSSs, titanium is used as inoculating addition (Ref 30-33). In as-cast B-bearing HSS, the addition of titanium can refine the solidification structure. The main reason is that titanium can combine with carbon in molten steel and form carbon compounds (TiC) having high melting point (Ref 34). According to the mismatch theory put forth by Turnbull (Ref 35), whether the high-melting compound can be non-spontaneous crystal nucleus of the new crystalline phase is determined by the mismatch of the two phases' lattice parameters:

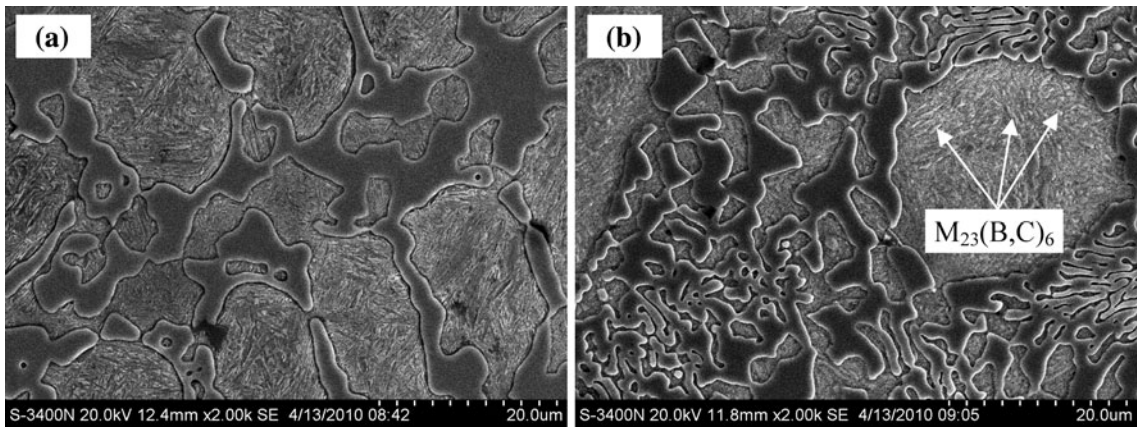

Fig. 5 SEM of B-bearing HSS tempered at 300 °C (a), and 500 °C (b)

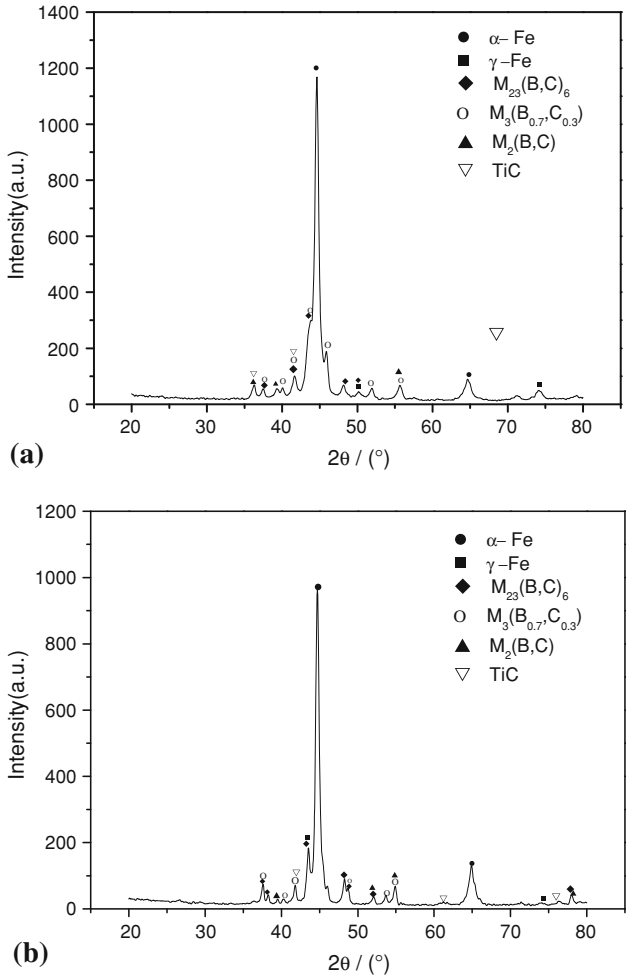

Fig. 6 XRD spectra of B-bearing HSS tempered at 300 °C (a), and 500 °C (b)

$$\delta = \frac{a_C - a_N}{a_N} \quad \text{(Eq 3)}$$

where, δ is the mismatch of lattice parameter; and a_C and a_N are the low-index planes of the substrate and the nucleated solid phase, respectively.

Bramfitt (Ref 36) proposed a theory stating that the nuclei were the most effective when the mismatch was under 6%, less effective between 6% and 12%, and become useless above 12%. TiC has high melting points and lower mismatch with γ-Fe lattice which is only 3.9%. Therefore, TiC can act as effective heterogeneous nuclei of primary austenite, and promote the refinement of the as-cast structure. Hence, the addition of titanium refined the austenite, hindered the coarsening of borocarbides during the solidification of B-bearing HSS, and promoted the occurrence of necking and broken network in the borocarbides. The macrohardness and impact toughness of the as-cast B-bearing HSS can reach up to 65-67 HRC and 80-85 kJ/m^2, respectively. The as-cast B-bearing HSS has higher hardness (65-67 HRC) and impact toughness (80-85 kJ/m^2) mainly because the addition of titanium leads to the refinement of solidification structure and the addition of boron leads to the hardening of matrix, which causes the increase of the hardness and impact toughness of the as-cast B-bearing HSS.

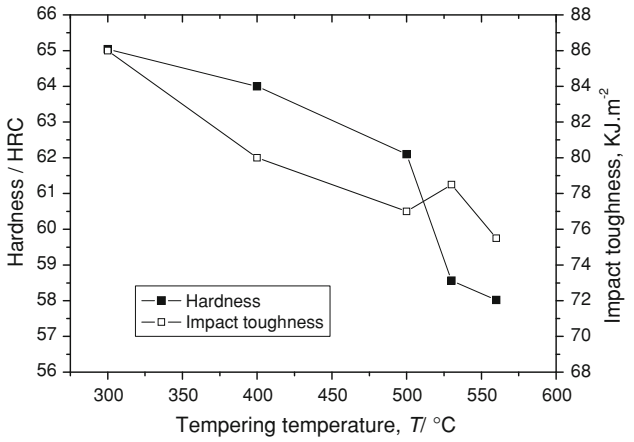

Fig. 7 Effect of tempering temperature on mechanical properties of B-bearing HSS

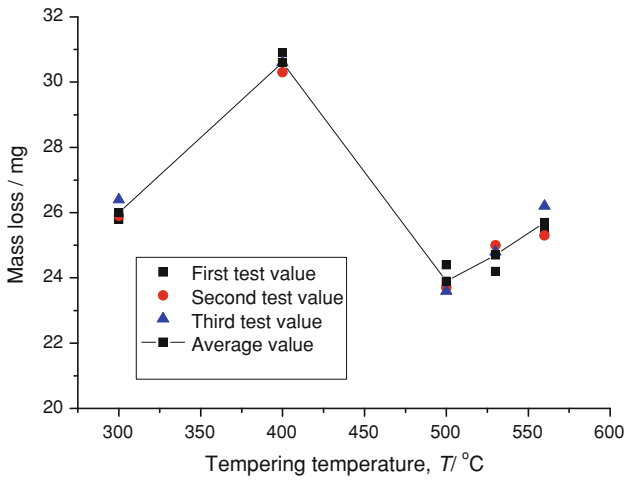

Fig. 8 Effect of tempering temperature on mass loss of B-bearing HSS

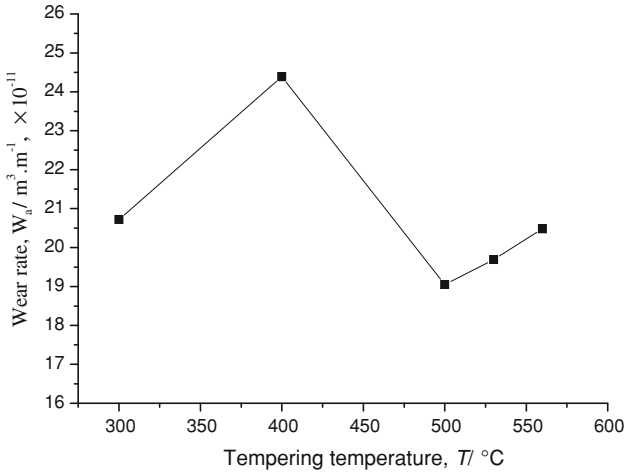

Fig. 9 Effect of tempering temperature on wear rate of B-bearing HSS

3.2 Effect of Tempering on Microstructure and Mechanical Properties of B-Bearing HSS

The matrix of as-cast B-bearing HSS consists of martensite and retained austenite and has higher hardness; the as-cast B-bearing HSS does not need quenching and can be directly used after tempering. The microstructures of B-bearing HSS tempered at different temperatures are shown in Fig. 5. The results of tempering test shows that the change of tempering temperature has no strong effect on eutectic borocarbides. However, there are many precipitated phases in the matrix after tempering, as shown in Fig. 5(b), and the amounts of precipitated phases increase with the increase of tempering temperature. XRD spectrum of tempered specimen confirms that precipitated phase is $M_{23}(B,C)_6$-type borocarbide, as shown in Fig. 6. Moreover, the retained austenite transforms into the martensite after tempering when tempering temperature excels 400 °C.

Effects of tempering temperature on mechanical properties of B-bearing HSS are shown in Fig. 7. When tempering temperature was lower than 500 °C, the hardness of B-bearing HSS decreased slightly with the increase of tempering temperature. When tempering temperature excelled 500 °C, the hardness decreased obviously. However, the change of tempering temperature had no obvious effect on impact toughness. When tempering temperature increases, the precipitation of fine borocarbide from the matrix leads to the decrease of solid solubilities of carbon, boron, tungsten, molybdenum, vanadium, chromium, etc. elements, which results in the decrease of

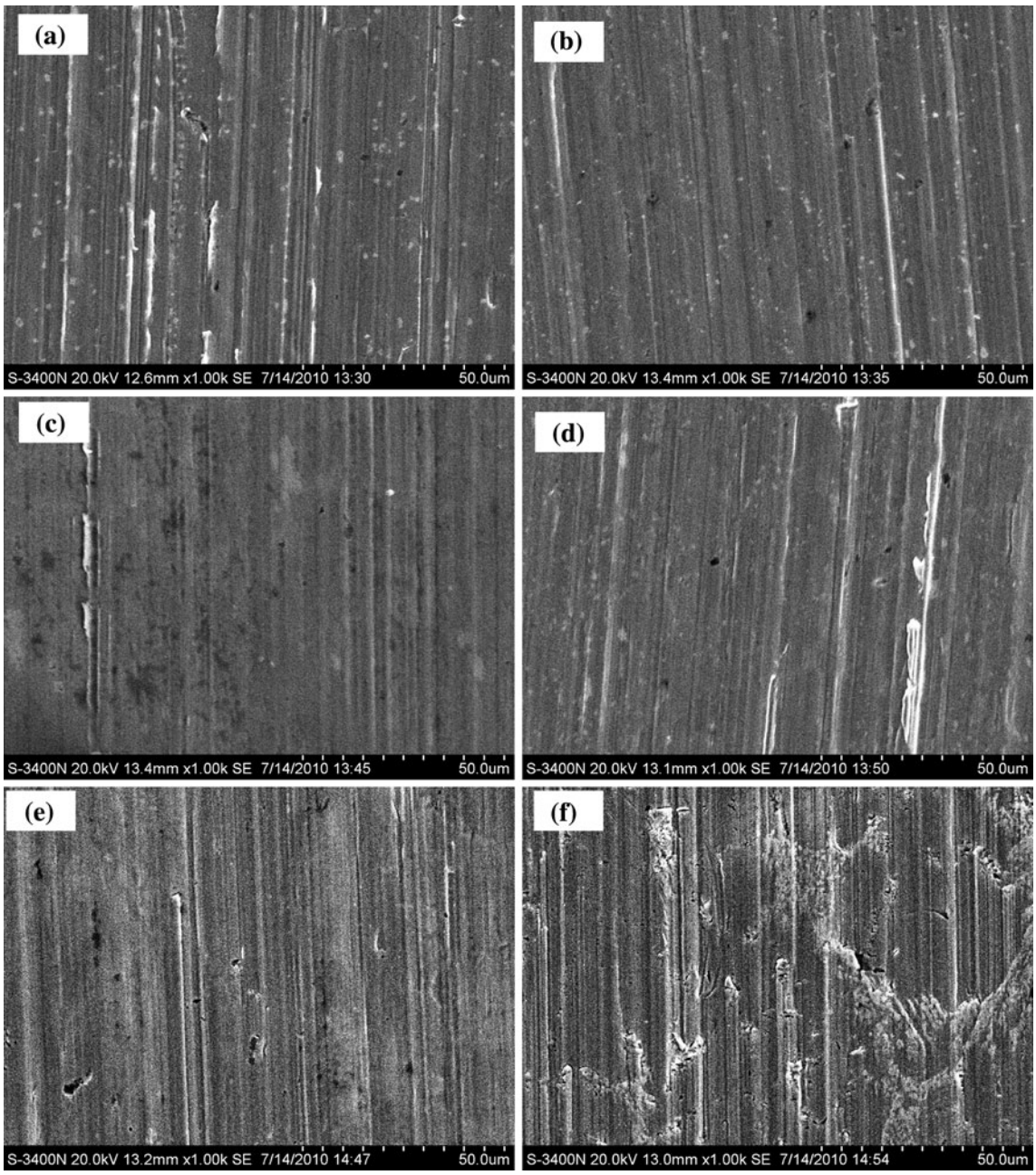

Fig. 10 Worn surface SEM image of B-containing HSS tempered at 300 °C (a), 400 °C (b), 500 °C (c), 530 °C (d), 560 °C (e), and high carbon HSS (f)

hardness. The change of tempering temperature has no obvious effect on impact toughness of B-bearing HSS mainly because of the combined action of the precipitating of borocarbide and the transformation of retained austenite. When tempering temperature is lower, retained austenite cannot be transformed, and there is no precipitating phase in martensitic matrix, and the impact toughness has no obvious change compared with as-cast B-bearing HSS. When tempering temperature is increased and reaches 500 °C, the supersaturated carbon and alloy elements separate out, and the carbon and alloy elements concentrations in the martensitic matrix decrease, which leads to the increase of impact toughness. However, higher tempering temperature accelerates the retained austenite transforming into the martensite, which leads to the decrease of impact toughness. The comprehensive result is that higher tempering temperature has no obvious effect on the impact toughness of B-bearing HSS. The hardness of cast B-bearing HSS tempered at 500 °C exceeds 62 HRC, and its impact toughness also exceeds 75 kJ/m^2. After tempering, the precipitation of borocarbide from the martensitic matrix led to the decrease of carbon and alloy elements' contents, which brought the decrease of as-tempered state hardness (about 58-62 HRC). Moreover, the retained austenite transformed into the martensite while tempering, which led to the decrease of tough phase and decreased the as-tempered state impact toughness (about 75-85 kJ/m^2).

3.3 Effect of Tempering on Wear Resistance of B-Bearing HSS

The effects of tempering temperature on the mass loss and wear rate of B-bearing HSS are shown in Fig. 8 and 9, respectively. Pin-on-disk abrasion test results show that the mass losses of B-bearing HSS tempered at 300, 400, 500, 530, and 560 °C are 26.0, 30.6, 23.9, 24.7, and 25.7 mg, respectively. Mass loss and wear rate of contrast specimen, viz. high-carbon high-vanadium HSS roll material, are 25.7 mg and 20.3×10^{-11} m^3/m, respectively, main compositions of which are 1.67%C, 5.08%Cr, 5.14%V, 5.09%Mo, 3.26%W, 2.88%Nb, and 1.04%Ni, and its hardness measured after quenching from 1050 °C and tempering at 525 °C is 62-64 HRC. The mass loss and wear rate of B-bearing HSS tempered at 500 °C are lower than those of high-carbon high-vanadium HSS, and its wear resistance is better than that of high-carbon high-vanadium HSS, which can be attributed to the effect of boron.

The pin-on-disk test belongs to two-body stationary abrasive wear, the micro-cutting model is the predominant wearing mechanism (Ref 37), in which the mass loss (wear resistance) of materials depends on their hardness. Moreover, the precipitated phase has also profitable effect on the wear of matrix (Ref 38). B-bearing HSS tempered at 500 °C has higher hardness, with a number of $M_{23}(B,C)_6$-precipitated phases in the matrix, which promotes the decrease of mass loss and the increase of wear resistance. The morphology of worn surface of Fig. 10 shows that the abrasion of B-bearing HSS tempered at 500 °C is lighter than those tempered at other temperatures, which affirms conclusively that B-bearing HSS tempered at 500 °C has better wear resistance.

4. Conclusions

(1) As-cast structure of B-bearing HSS consisted of α-Fe, $M_{23}(B,C)_6$-, $M_3(B_{0.7}C_{0.3})$-, and $M_2(B,C)$-type borocarbides, a small quantity of retained austenite and small amount of TiC.

(2) There were many $M_{23}(B,C)_6$-precipitated phases in the matrix after tempering.

(3) Hardness of cast B-bearing HSS tempered at 500 °C exceeds 62 HRC, and its impact toughness also exceeds 75 kJ/m^2. B-bearing HSS tempered at 500 °C has excellent wear resistance, which can be attributed to the effect of boron.

Acknowledgments

The authors would like to acknowledge the financial support for this study from the National Natural Science Foundation of China under grant (51274016) and the Scientific Plan Item of Beijing Education Committee under grant (PXM2012-136, PXM2012-156).

References

1. P.R. Da Mota, R.A. Goncalves, A.M. Reis, and M.B. Da Silva, Performance of High-Speed Steel Taps at High Cutting Speed, *Int. J. Mach. Mach. Mater.*, 2007, **2**(2), p 299–308
2. A.S. Chaus, M.V. Sitkevich, and P. Pokorný, Cutting Tests for End-Milling Radius Cutters of High-Speed Steel With and Without Diffusion Coating, *J. Frict. Wear*, 2010, **31**(6), p 419–425
3. M. Andersson, R. Finnstrom, and T. Nylen, Introduction of Enhanced Indefinite Chill and High Speed Steel Rolls in European Hot Strip Mills, *Ironmaking Steelmaking*, 2004, **31**(5), p 383–388
4. H.G. Fu, Y.H. Qu, J.D. Xing, X.H. Zhi, Z.Q. Jiang, M.W. Li, and Y. Zhang, Investigations on Heat Treatment of a High-Speed Steel Roll, *J. Mater. Eng. Perform.*, 2008, **17**(4), p 535–542
5. N.F. Garza-Montes-de-Oca and W.M. Rainforth, Wear Mechanisms Experienced by a Work Roll Grade High Speed Steel Under Different Environmental Conditions, *Wear*, 2009, **267**(1-4), p 441–448
6. R.R. Xavier, M.A. de Carvalho, E. Cannizza, T.H. White, Jr., and A. Sinatora, High-Speed Steel Rolls for Long Products, *Iron Steel Technol.*, 2004, **1**(2), p 28–33
7. B.C. Hwang, D.W. Suh, and S.J. Kim, Austenitizing Temperature and Hardenability of Low-Carbon Boron Steels, *Scr. Mater.*, 2011, **64**(12), p 1118–1120
8. J.J. Zhang, Y.M. Gao, J.D. Xing, S.Q. Ma, D.W. Yi, L. Liu, and J.B. Yan, Effects of Plastic Deformation and Heat Treatment on Microstructure and Properties of High Boron Cast Steel, *J. Mater. Eng. Perform.*, 2011, **20**(9), p 1658–1664
9. J.W. Li, S. Zhang Guo, S.Z. Wei, and Q. Zhao, Preparation Technology of the Low Carbon High Boron Fe-C-B Wear Resistance Steel, *Appl. Mech. Mater.*, 2011, **52-54**, p 1718–1722
10. P.F. Wu, X.D. Liu, G.D. Che, Y. Lu, J.M. Wang, and J.F. Li, Effects of Heat-Treatment Process on Mechanical Properties and Microstructure of $ZG_{30}Cr_2Mn_2Si$, *Foundry China*, 2008, **57**, p 63–65
11. Z.Q. Jiang, H.G. Fu, J. Yang, and J.H. Wang, Effect of Quenching Temperature on Microstructure and Hardness of High Boron Cast Steel, *Trans. Mater. Heat Treat.*, 2007, **28**, p 158–160
12. K. Weber, D. Regener, H. Mehner, and M. Menzel, Characterization of the Microstructure of High-Chromium Cast Irons Using Mössbauer Spectroscopy, *Mater. Charact.*, 2001, **46**, p 399–406
13. C.P. Tabrett and I.R. Sare, The Effect of Heat Treatment on the Abrasion Resistance of Alloy White Irons, *Wear*, 1997, **203-204**, p 206–219
14. L.E. Zevin and G. Kimmel, *Quantitative X-Ray Diffractometry*, Springer, New York, 1995
15. C.M. Kim, X-Ray Method of Measuring Retained Austenite in Heat Treated White Cast Irons, *J. Heat. Treat.*, 1979, **1**, p 43–51
16. F. Xiong, *Metallography of X-Ray*, Machinery Industry Press, Beijing, 1981
17. B. Wanzhen, W. Shizhong, L. Rui, X. Liujie, D. Zhanwu, and Y. Xiong, Effects of Retained Austenite on Rolling Wear Properties of

High Vanadium High Speed Steel, *Lubr. Eng.*, 2007, **32**, p 66–72 (In Chin.)
18. Measurement of Retained Austenite in the Steel—X-ray Diffractometer Method. GB8362-1987
19. Q.S. Luo, J.P. Xie, and Y.P. Song, Effects of Microstructures on the Abrasive Wear Behaviour of Spheroidal Cast Iron, *Wear*, 1995, **184**(1), p 1–10
20. H.G. Fu, Q. Xiao, and J.D. Xing, A Study of Microstructure and Performance of Tempered Fe-V-W-Mo Alloy, *Steel Res. Int.*, 2006, **77**(2), p 139–143
21. J.D. Xing, W.H. Lu, and X.T. Wang, *Proceedings of International Conference on Wear of Materials*, Reston, VA, April 11-14, 1983, K.C. Ludema, Ed., ASME, New York, 1983, p 45
22. H.M. Wang and J.L. Ji, Wear Behaviour of CTC I, FeCrCSi Composite, *Chin. J. Met. Sci. Technol.*, 1990, **6**, p 357–364
23. A.Y. Mosbah, D. Wexler, and A. Calka, Abrasive Wear of WC-FeAl Composites, *Wear*, 2005, **258**, p 1337–1341
24. G. Abbas and U. Ghazanfar, Two-Body Abrasive Wear Studies of Laser Produced Stainless Steel and Stainless Steel + SiC Composite Clads, *Wear*, 2005, **258**, p 258–264
25. H.G. Fu, Y.P. Lei, J.D. Xing, and L.M. Huang, Investigations on Microstructures and Properties of B containing Cast Steel for Wear Resistance Applications, *Ironmaking Steelmaking*, 2008, **35**(5), p 371–378
26. H.M. Wang, Q. Zhang, and H.S. Shao, Two-Body Abrasive Wear Behaviour of Austempered Steel, *Wear Theory and Anti-Wear Technology*, F.Y. Lin, Ed., Science Press, Beijing, 1993, p 162–165
27. C.K. Kim, D.G. Lee, and S. Lee, Correlation of Microstructure and Fracture Properties of Five Centrifugal Cast High Speed Steel Rolls, *Mater. Sci. Technol.*, 2007, **23**(9), p 1065–1074
28. X. Li, Z. Du, H. Fu, Z. Feng, and H. Zhao, Experimental Investigation on Heat Treatment of a High-Speed Steel for Hot Rolling Roll Mill, *Materialwiss. Werkstofftech.*, 2010, **41**(3), p 170–176
29. H. Baker, *Alloy Phase Diagrams, vol. 3 of ASM Handbook*, ASM International, Materials Park, OH, 1992, p 281
30. A.S. Chaus, Modifying Cast Tungsten-Molybdenum High-Speed Steels with Niobium, Zirconium, and Titanium, *Met. Sci. Heat Treat.*, 2005, **47**(1-2), p 53–61
31. A.S. Chaus and F.I. Rudnitskii, Effect of Modification on the Structure and Properties of Cast Tungsten-Molybdenum High-Speed Steels, *Met. Sci. Heat Treat.*, 1989, **31**(1-2), p 121–128
32. S. Kheirandish, Effect of Ti and Nb on the Formation of Carbides and the Mechanical Properties in As-Cast AISI-M7 High-Speed Steel, *ISIJ Int.*, 2001, **41**, p 1502–1509
33. S. Kheirandish, S. Mirdamadi, and Y.H.K. Kharrazi, Effect of Titanium on Cast Structure of High Speed Steel, *Mater. Sci. Technol.*, 1998, **14**, p 312–316
34. H.G. Fu, D.M. Fu, D.N. Zou, and J.D. Xing, Structures and Properties of High-Carbon High Speed Steel by RE-Mg-Ti Compound Modification, *J. Wuhan Univ. Technol. Mater. Sci. Ed.*, 2004, **19**(2), p 48–51
35. D. Turnbull and B. Vonnegut, Nucleation Catalysis, *Ind. Eng. Chem.*, 1952, **44**(6), p 1292–1298
36. B.L. Bramfitt, Planar Lattice Disregistry Theory and Its Application on Heterogistry Nuclei of Metal, *Metall. Trans.*, 1970, **1**(7), p 1987–1995
37. M.M. Khruschov, The Effect of Wear on the Compressive Stress in the Sphere on Plane Configuration, *Wear*, 1974, **28**, p 69–78
38. S. Hesheng and Z. Qing, *Abrasive Wear of Metal and Wear-Resistant Materials*, Machinery Industry Press, Beijing, 1988